galaxies

MDPI

Review

From the *s*-Process to the *i*-Process: A New Perspective on the Chemical Enrichment of Extrinsic Stars

Sophie Van Eck [1,2,*], Riano Giribaldi [1], Thibault Merle [1,2,3], Adrian Lambotte [1], Drisya Karinkuzhi [4], Stéphane Goriely [1,2], Arthur Choplin [1,2], Nicholas Storm [5,6], Jeffrey Gerber [7], Lionel Siess [1,2], Maria Bergemann [5] and Alain Jorissen [1,2]

1 Institut d'Astronomie et d'Astrophysique, Université libre de Bruxelles, CP 226, B-1050 Brussels, Belgium; rianoesc@gmail.com (R.G.); thibault.merle@ulb.be (T.M.); adrian.lambotte@ulb.be (A.L.); stephane.goriely@ulb.be (S.G.); arthur.choplin@ulb.be (A.C.); lionel.siess@ulb.be (L.S.); alain.jorissen@ulb.be (A.J.)
2 BLU-ULB, Brussels Laboratory of the Universe, B-1050 Brussels, Belgium
3 Royal Observatory of Belgium, Avenue Circulaire 3, B-1180 Brussels, Belgium
4 Department of Physics, University of Calicut, Malappuram 673635, India; drisyadev@gmail.com
5 Max-Planck-Institut für Astronomie, Königstuhl 17, 69117 Heidelberg, Germany; storm@mpia.de (N.S.); bergemann@mpia-hd.mpg.de (M.B.)
6 Heidelberg Graduate School for Physics, Grabengasse 1, 69117 Heidelberg, Germany
7 Department of Physics and Astronomy, Purdue University, West Lafayette, IN 47907, USA; gerber48@purdue.edu
* Correspondence: sophie.van.eck@ulb.be

Abstract: Separating stars enriched in the *s*- and *r*-processes of nucleosynthesis is usually achieved by analyzing the element ratios of *s*-process elements (like Ba or La) to *r*-process elements (like Eu). The situation becomes more complex when analyzing CEMP-rs stars, which are carbon-enriched metal-poor objects enriched in a mixture of s- and r-elements. These objects, possibly resulting from the *i*-process of nucleosynthesis, are notoriously difficult to classify based on elemental ratios. Recent theoretical studies have outlined, however, that the *s*-, *i*-, and *r*-processes produce distinct isotopic mixtures. Here, we propose to analyze a sample of stars known to be enriched in s, r, or r + s elements and to determine the odd-to-even isotopic ratio measured on atomic lines of barium, in order to validate or disprove their assignation.

Keywords: nucleosynthesis; metal-poor stars; *i*-process

Citation: Van Eck, S.; Giribaldi, R.; Merle, T.; Lambotte, A.; Karinkuzhi, D.; Goriely, S.; Choplin, A.; Storm, N.; Gerber, J.; Siess, L.; et al. From the *s*-Process to the *i*-Process: A New Perspective on the Chemical Enrichment of Extrinsic Stars. *Galaxies* **2024**, *12*, 89. https://doi.org/10.3390/galaxies12060089

Academic Editors: Oscar Straniero and Oleg Malkov

Received: 26 September 2024
Revised: 12 December 2024
Accepted: 16 December 2024
Published: 23 December 2024

1. Introduction

Elements heavier than iron are produced by neutron captures on iron-seed nuclei, either by the *s*-process (for 'slow'), or by the *r*-process (for 'rapid'), leaving aside the marginal contribution by the *p*-process [1]. The *s*-process proceeds at neutron densities of the order of $\sim 10^8$ cm^{-3} and builds up isotopes close the valley of nuclear stability [2–4], whereas the *r*-process, which produces more neutron-rich isotopes, occurs at typical neutron densities in excess of $\sim 10^{20}$ cm^{-3} [5,6].

- The site of the *s*-process for $A > 90$ nuclei is well-identified as low- and intermediate-mass ($M \lesssim 3 - 4M_{\odot}$) thermally-pulsing asymptotic giant branch (TP-AGB) stars [3,4,7,8]. Stars producing their *s*-process elements are classified as intrinsic S or carbon stars, whereas stars polluted by *s*-process material originating from a companion are tagged extrinsic S, barium, CH, or CEMP-s stars (CEMP stands for 'carbon-enriched metal-poor'), by order of decreasing metallicity.
- The site of the *r*-process is still debated: the decompression of neutron–star matter ejected during a binary neutron star merger [9] provides, since the observation of GW170817 [10], a promising alternative to core-collapse supernovae [11] or magnetorotational supernovae (e.g., [12]). Whether the neutron star merger site is

the only one contributing to the *r*-process is still highly debated [13,14]. *r*-process-enriched stars are found among the CEMP-r stellar class, subdivided into the classes r-I ($0.3 < [Eu/Fe] < 0.7$ and $[Ba/Eu] < 0$), r-II ($[Eu/Fe] > 0.7$ and $[Ba/Eu] < 0$), and r-III ($[Eu/Fe] > 2$) ([15] and references therein). We adopt the usual notation: $[A/B] = \log_{10}(N_A/N_B)_* - \log_{10}(N_A/N_B)_\odot$, where N_X is the number density of the X element and $\epsilon_x = \log_{10}(N_X/N_H) + 12$.

- Some stars are enriched in both r- and s-elements; they are also carbon-enriched and have been initially detected among metal-poor stars (they are thus tagged CEMP-rs) and among CH stars. However, some of them have been found in more metal-rich ($[Fe/H] = -0.5$) carbon-enriched objects (see e.g., [16–20]).

The current criteria used to distinguish CEMP-rs from CEMP-s stars are based on [Ba/Eu] or [La/Eu] ratio [21,22] or on a series of (first and second-peak) *s*- and *r*-elemental abundances [18,23]. However, the boundary between the two classes is somewhat empirical and depends on the discriminating criteria, and a robust identification scheme is difficult to define [18]. Both CEMP-s and CEMP-rs stars seem to belong to binary systems ([24] and references therein), so binarity cannot be used as a discriminant.

The origin of the peculiar abundance patterns in stars showing enhancements in both *s*- and *r*-process elements is still an open question ([21,22,25] and references therein). Several exotic scenarios have been mentioned to explain the hybrid abundance profile of CEMP-rs stars, in particular primordial origin (pollution of the birth cloud by an *r*-process source), pollution of the binary by a third massive star (triple system) ([26] and references therein), pollution by the primary exploding as a type 1.5 supernova or accretion-induced collapse [22,26–28], or the *i*-process (for 'intermediate-process') scenario [29,30]. The latter operates at neutron densities of the order of $\sim 10^{14-15}$cm^{-3}, intermediate between those of the *s*- and *r*-processes. Recently, the abundances of CEMP-rs stars have been explained (as satisfactorily as those of the *s*-process) by low-metallicity ($[Fe/H] \sim -2.5$) $1-2$ M$_\odot$ AGB models experiencing proton ingestion [18,31,32]. According to this scenario, during a thermal pulse at the beginning of the TP-AGB, the He-driven convection zone penetrates in the H-rich layer. The subsequent proton ingestion leads to the production of ^{13}C from the ^{12}C(p,γ)^{13}N(β)^{13}C chain of reactions and, consequent to a strong neutron burst, via the ^{13}C(α,n)^{16}O reaction, with neutron densities adequate for the synthesis of elements heavier than iron. Exotic or hybrid sites for the *i*-process might therefore not be required.

Different isotopic mixtures are predicted for the *s*-process, and for the *r*- or *i*-processes. The *s*-process mainly produces the even-N isotopes due to the strong even–odd and shell effects affecting the isotopic abundances (directly in line with the local equilibrium, i.e., a constant $N(A)\langle\sigma\rangle_A$ along an isotopic chain, where $N(A)$ is the abundance of isotope A and $\langle\sigma\rangle_A$ its Maxwellian-averaged neutron capture cross section). The *i*-process is also expected to be sensitive to similar effects but on the progenitors along the Cs and I chains, with a negligible production of the shielded ^{134,136}Ba and a weak production of ^{135}Ba due to the long half-life of ^{135}I of 6.6 h. In the case of the *r*-process, ^{134,136}Ba cannot be produced and a rather similar production of the other Ba isotopes is found, the odd–even effect being washed out by statistical averaging on a large number of physical irradiation conditions and the impact of smoothing effects like β-delayed neutron emission [5].

Such a disparity in the isotopic mixture can be well represented by the barium even-to-odd isotope abundance ratio $f_{\rm Ba,odd} = (N(^{135}{\rm Ba}) + N(^{137}{\rm Ba}))/N({\rm Ba})$. Based on astrophysical as well as nuclear physics uncertainties affecting the s- [4] and *i*-processes [33,34] in AGB stars, we have estimated the predicted range of the $f_{\rm Ba,odd}$ ratio. Values of $f_{\rm Ba,odd} \simeq 0.10 \pm 0.03$ are obtained for an *s*-process origin and $f_{\rm Ba,odd} = 0.67^{+0.09}_{-0.40}$ [35] for the *i*-process. In the case of the *r*-process, significant nuclear and astrophysical uncertainties remain, so that modeling is difficult to use nowadays to infer an *r*-process pollution. However, since many r-II stars have been shown to follow the same pattern as the solar r-distribution [6], it can be assumed that $f_{\rm Ba,odd}$ follows the solar r-ratios and their corresponding uncertainties stemming from solar abundance determination, as well as nuclear

and astrophysics modeling of the *s*-process [36–38]. With this assumption, we obtain the *r*-process value of $f_{\mathrm{Ba,odd}} = 0.66 \pm 0.20$.

Isotopic abundances are notoriously difficult to measure from atomic lines because isotopic shifts (a few mÅ) are negligible compared to the line width. However, in contrast with the spectral lines of even isotopes, the lines of the odd isotopes are affected by hyperfine splitting (HFS), the effect of which can be larger than $\sim$ 50 mÅ. It is thus possible to measure $f_{\mathrm{Ba,odd}}$ and to relate it to a given nucleosynthetic process (either *s*-process or *i*/*r*-processes). After the pioneering studies of [39–42], this technique has been applied in [43–47], with contradictory conclusions. Indeed, the subgiant used in these studies, HD 140283, had weak Ba lines, and the non-local thermodynamic equilibrium (NLTE) effects were not taken into account. Only a handful of measurements are available from high-resolution high-S/N spectra analyzed in NLTE conditions in CEMP stars, as summarized in Table 1.

Table 1. Literature review of non-local thermodynamic equilibrium (NLTE) and 3D Ba odd-to-even measurements. LTE and NLTE apply to the fitting of the barium lines.

Star ID	Type	[Fe/H]	$f_{\mathrm{Ba,odd}}$	LTE/NLTE	R	SNR	Ref.
HE 0338-3945	CEMP-rs	−2.42	0.23 ± 0.12	NLTE	35,000	≥70	[48]
CS 31082-001	CEMP-rII	−2.90	0.43 ± 0.09	NLTE	75,000	≥250	[48]
CS 29491-069	CEMP-rII	−2.58	0.46 ± 0.08	NLTE	60,000	70–50	[49]
HE 1219-0312	CEMP-rII	−2.94	0.51±0.09	NLTE	70,000	110–111	[49]
HE 2327-5642	CEMP-rII	−2.87	0.50±0.13	NLTE	60,000	50–100	[49]
HE 2252-4225	CEMP-rII	−2.67	0.48±0.12	NLTE	50,000	70–60	[49]
HD 140283	CEMP-rI	−2.50	0.38 ±0.1	3D, LTE	95,000	1100 *	[47]

* S/N per 12 mÅ wide pixel around 4500 Å.

It has been confirmed [39–42,50] that the 4554 Å Ba II resonance line (used to measure $f_{\mathrm{Ba,odd}}$) is formed under NLTE conditions in metal-poor stars. Ba isotopic fractions in CEMP-r-II stars were first reported by [48], who found that the $f_{\mathrm{Ba,odd}}$ value in CS 31082-001 is consistent with the isotopic ratio in the solar pure *r*-process component. We note, however, that the result of [48] ($f_{\mathrm{Ba,odd}} = 0.23 \pm 0.12$) for the CEMP-rs object HE0338-3945 is incompatible with [31] the model predictions for the *i*-process at low metallicity ($f_{\mathrm{Ba,odd}} \simeq 0.53$) for the *r*-process ($f_{\mathrm{Ba,odd}} \simeq 0.66$) and marginally compatible with an *s*-process occurring in a metal poor star ($f_{\mathrm{Ba,odd}} \simeq 0.10$).

2. Isotopic Ratio Determination

2.1. Materials and Methods

Our star sample consists of three stars known, to the best of today's knowledge, to have abundance profiles corresponding to three distinct nucleosynthesis processes, as shown in Table 2. For two of them, we obtained spectra from the HERMES spectrograph mounted on the 1.2 m Mercator telescope [51] installed on the Roque de los Muchachos Observatory (Canary Islands, Spain). The spectral resolution is 86,000, with a spectral range spanning 3800 to 9000 Å. The signal-to-noise ratio has been enhanced by co-adding multiple exposures. We also included in our analysis two ESO-UVES archive spectra of the star HE 2208-1239, with a wavelength range of 4780–6800 Å (resp., 3300–4515 Å), a resolution of $R = 56{,}990$ (resp., R = 49,620), and an SNR of 100 (resp., 40).

Table 2. Sample stars.

Star	Type	Reference	Spectrograph	SNR
HD 2454	Dwarf Ba (s)	[52]	HERMES	330
HD 115444	CEMP-r	[53]	HERMES	350
HE 2208-1239	CEMP-r/s	[54]	UVES	40–100

The stellar parameters were derived as follows: the effective temperature was determined by fitting selected regions of the H_α line profile wings, following the method of [55–57]. Surface gravity was obtained by fitting the wings of the Mg Ib triplet at 5171 and 5183 Å, as described in [57]. Metallicity and microturbulence were derived jointly by ensuring no correlation between iron abundance and the reduced equivalent width of the lines. In this process, iron abundance was determined using the NLTE Turbospectrum radiative transfer code [58]. The parameters were iterated until the effective temperature, surface gravity, metallicity, and microturbulence were simultaneously fitted by the aforementioned methods. The resulting parameters are presented in Table 3.

Table 3. Atmospheric parameters of the sample stars.

Star	$T_{\rm eff}$ (K)	$\log g$ (dex)	[Fe/H]$_{NLTE}$ (dex)	v_{mic}^{NLTE} (km/s)	$v_{mic}^{\rm Ba}$ (km/s)
HD 2454	6565 ± 21	4.11 ± 0.06	-0.21 ± 0.05	1.60 ± 0.20	not required
HD 115444	4667 ± 86	1.28 ± 0.15	-2.97 ± 0.08	1.40 ± 0.15	$1.65^{+0.45}_{-0.30}$
HE 2208-1239	5200 ± 75	2.14 ± 0.15	-2.40 ± 0.09	0.85 ± 0.20	2.15 ± 0.15

This procedure yielded an unexpected outcome: the barium abundances derived from the three subordinate Ba lines (5853.67, 6141.71, and 6496.90 Å; subordinate lines denote lines that correspond to transitions from one excited state to another excited state) did not align with those from two resonance Ba lines (4554.03 and 4934.08 Å). The subordinate lines provided abundances that were, on average, 0.7 dex higher (except for HD 2454). This discrepancy is likely due to the fact that 1D model atmospheres cannot provide a consistent microturbulence value that fits both the moderate (subordinate) and strong (resonance) barium lines simultaneously. In an upcoming study, 3D model atmospheres will be used for the analysis of the three stars. In the meantime, a reasonable assumption was tested: adopting the same barium abundance relative to solar as that of its neighboring element cerium, namely: $[{\rm Ba/Fe}]_* = [{\rm Ce/Fe}]_*$. Since the abundance is no longer a free parameter, the value of the microturbulence must be adapted, in order to be able to fit the three barium subordinate lines.

Despite its simplicity, this assumption led to remarkably consistent results for the isotopic fractions, as demonstrated below.

2.2. Results

Figure 1 shows the fits of the Ba II resonance line at 4934.08 Å. The best fit, determined from the smallest residuals, is highlighted in violet across all panels. The barium isotopic fraction, $f_{\rm odd}^{\rm Ba}$, is derived by finding the best match between the synthetic spectra, obtained by varying $f_{\rm odd}^{\rm Ba}$, and the observed spectrum, as quantified by the minimum normalized χ^2 (see insets in each panel of Figure 1).

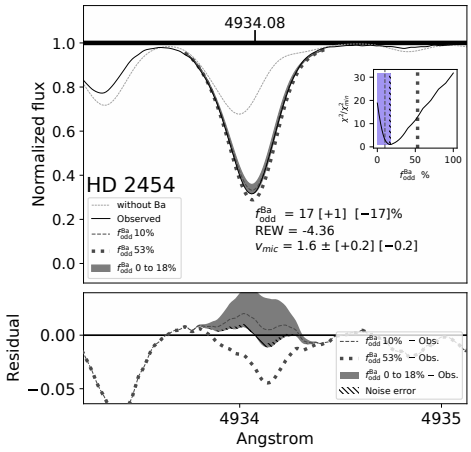

Figure 1. *Cont.*

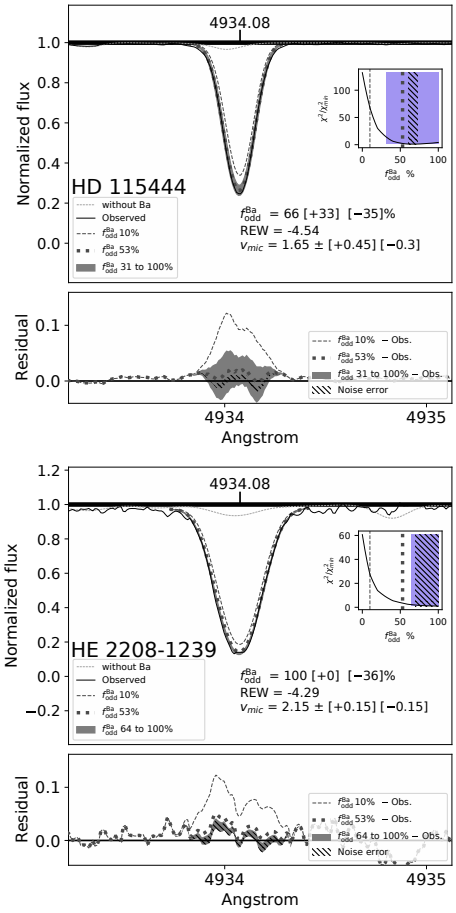

Figure 1. Fits to the 4934.08 Å Ba II resonance line for the three sample stars. The thin black line represents the observed spectrum, while the dashed, dotted, and thick violet lines represent the spectral synthesis with different $f^{\mathrm{Ba}}_{\mathrm{odd}}$, as labeled (the 10% dashed line characterizing an *s*-process origin and the 53% thick-dashed line an *i*-process). The thin dashed line shows a spectral synthesis without barium. The lower panels display residuals for each fit shown in the upper panels. The fits with smaller residuals are highlighted in grey. The barium isotopic fraction, $f^{\mathrm{Ba}}_{\mathrm{odd}}$, is determined by identifying the best agreement between the synthetic spectra (for varying $f^{\mathrm{Ba}}_{\mathrm{odd}}$) and the observed spectrum, as quantified by the minimum normalized χ^2 illustrated in the upper right inset of each panel.

As noted in the Introduction, each nucleosynthesis process (*s*-, *r*- and *i*-processes) corresponds to a distinct isotopic fraction ($f^{\mathrm{Ba}}_{\mathrm{odd}} \simeq 0.10, 0.66, 0.53$, respectively), based on nucleosynthesis calculations. Our results (Figure 1) support the classification found in the literature and reported in Table 2, namely: the *s*-process origin for HD 2454 (consistent with its classification as a dwarf Barium star), and *i*- or *r*-processes nature for the CEMP-r/s stars HE 2208-1239 and the CEMP-r star HD 115444. However, distinguishing between the *i*- and *r*-processes is not possible based solely on the barium isotopic fraction.

This assignation is further validated using the criteria for distinguishing CEMP-s, -r, and -r/s stars established in [18], where we compute a signed distance:

$$d_S = \frac{1}{N}\sum_{x_i}(\log_{10}\epsilon_{x_i,*} - \log_{10}\epsilon_{x_i,\mathrm{norm(r,*)}}) \quad (1)$$

and an RMS distance to the *r*-process

$$d_{\mathrm{RMS}} = \left(\frac{1}{N}\sum_{x_i}(\log_{10}\epsilon_{x_i,*} - \log_{10}\epsilon_{x_i,\mathrm{norm(r,*)}})^2\right)^{1/2} \quad (2)$$

where $\{x_1 \dots x_N\}$ is the list of the N considered heavy elements, and we use the usual notation $\log_{10}\epsilon_{x_i} = \log_{10}(n_{x_i}/n_H) + 12$, with n_{x_i} as the number density of element x_i. We denote $\log_{10}\epsilon_{x_{i,*}}$ the abundance of element x_i as measured in the stars, and $\log_{10}\epsilon_{x_i,\mathrm{norm(r,*)}}$ the standard r-process abundance profile $\log_{10}\epsilon_{x_i,r}$ normalized to the star abundance profile with respect to europium: $\log_{10}\epsilon_{x_i,\mathrm{norm(r,*)}} = \log_{10}\epsilon_{x_i,r} + (\log_{10}\epsilon_{\mathrm{Eu},*} - \log_{10}\epsilon_{\mathrm{Eu,r}})$. The adopted standard r-process abundances ($\log_{10}\epsilon_{x_i,r}$) are listed in Table B.4 of [18]. We selected europium as a normalizing element because it is mainly produced by the r-process and is easily measurable in most stars. Here, we consider the element set x_i = {Y, Zr, Ba, La, Ce, Nd, Sm} (and Eu for normalization).

The dividing threshold between the CEMP-r/s and CEMP-s stars was fixed at $d = 0.7$ for both distances [18].

Additionally, we computed the χ^2 differences between the measured abundances and those predicted by either the s- or the i-process models [4,32].

$$\chi^2 = \frac{1}{N_{\mathrm{obs}}} \sum_X \frac{([\mathrm{X/Fe}]_{\mathrm{obs}} - [\mathrm{X/Fe}]_{\mathrm{mod}})^2}{\sigma^2_{X,\mathrm{obs}}} \quad (3)$$

where N_{obs} is the total number of data points for a given star. The $\chi^2_{\mathrm{r-pro}}$ values reported in Table 4 are derived considering all elements with $Z > 30$. For HD 2454 and HE 2208-1239, the $\chi^2_{\mathrm{s-pro}}$ and $\chi^2_{\mathrm{i-pro}}$ values are based on all available elements of Giribaldi (2024, in prep.), including light ones (16 for HD 2454 and 15 for HD 2208-1239). For the likely r-process star HD 115444, only $Z > 30$ elements (13 in total) are considered to compute $\chi^2_{\mathrm{s-pro}}$ and $\chi^2_{\mathrm{i-pro}}$. The results are summarized in Table 4.

Table 4. Summary of the nucleosynthetic process indicators.

Star	Type	Signed Distance	RMS Distance	$\chi^2_{\mathrm{s-pro}}$	$\chi^2_{\mathrm{i-pro}}$	$\chi^2_{\mathrm{r-pro}}$	f^{Ba}_{odd}
HD 2454	Dwarf Ba (s)	0.83	0.90	1.38	1.56	4.47	17^{+1}_{-17}
HD 115444	CEMP-r	0.00	0.14	4.46	2.35	0.79	66^{+33}_{-35}
HE 2208-1239	CEMP-r/s	0.56	0.80	13.14	2.05	7.37	100^{+0}_{-36}

The conclusions for the three investigated stars are as follows:

- HD 2454: Both the signed and RMS distances exceed 0.7, indicating that the s-process is responsible for the measured chemical peculiarities. The χ^2 analysis also strongly supports the s-process. Furthermore, the low value of $f^{Ba}_{\mathrm{odd}} = 17^{(+1-17)}\%$ is consistent only with the s-process.
- HD 115444: The signed and RMS distances are very small or even zero, as expected for a pure r-process abundance profile. The χ^2 analysis also favors the r-process. The isotopic fraction $f^{Ba}_{\mathrm{odd}} = 66^{(+33-35)}\%$ rules out the s-process but cannot distinguish between pollution by an i- or r-process.
- HE 2208-1239: The signed distance is below the threshold of 0.7, pointing to an i-process, while the RMS distance suggests the s-process. The χ^2 analysis offers a clearer conclusion, strongly supporting the i-process, likely due to the inclusion of more chemical elements. Finally, $f^{Ba}_{\mathrm{odd}} = 100^{(+0-36)}\%$ suggests an i- or r-process origin.

In conclusion, the barium isotopic ratio alone can reliably identify an s-process but cannot discriminate well between an i- or r-process origin. To resolve this, another isotopic fraction, such as the one of europium, could be considered. However, when combined with additional independent indicators like d_S or d_{RMS}, which compare individual abundances to a reference abundance profile, a consistent diagnostic emerges, with all indicators aligning. The assumption of adopting a barium abundance similar to that of cerium, though initially strong, appears reasonable in retrospect.

3. Extrinsic Stars in Surveys: Searching for a Needle in a Haystack

Stars exhibiting anomalous chemical abundance patterns in carbon or heavy elements (such as Barium, CH, and CEMP stars) were primarily discovered through low-resolution surveys, including prism-objective surveys, conducted in the last century. With the advent of medium- and high-resolution surveys, it is now feasible to compile new catalogues of extrinsic stars with significantly more members and reduced biases, sometimes using machine learning techniques. However, caution is warranted when using automated methods to detect anomalous objects. In [20], 15 objects previously identified as enriched in strontium using low-resolution spectra were re-analyzed. This study found that four of these objects actually had normal strontium abundances; the misclassification was due to an unrecognized blend with a CN band head. Therefore, it is crucial to validate machine-learning results with classical methods.

In [59], cerium abundances were determined from Gaia RVS spectra using the GSP-Spec module. As expected, most cerium-enriched objects are found on the asymptotic giant branch, at $T_{\rm eff} < 3800$K. Interestingly, a subpanel of their Figure 3, which shows a Kiel diagram ($\log g$, $T_{\rm eff}$) color-coded with Ce abundance, reveals a group of cerium-enriched stars located at $2.5 < \log g < 3.5$ and 4500 K $< T_{\rm eff} <$ 5500 K, as shown in Figure 2.

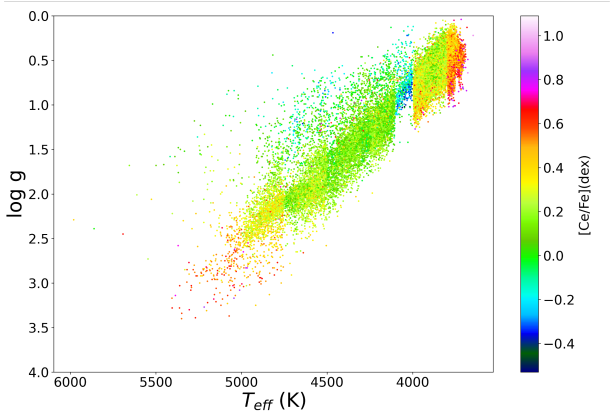

Figure 2. Kiel diagram of stars from the Gaia catalogue, having a reliable GSP-Spec cerium abundance (as color-coded), as in [59].

From the GAIA data with GSP-Spec cerium abundances, we selected a sample of 82 extrinsic star candidates having [Ce/Fe] > 0.6 dex and 4500 K $< T_{\rm eff} <$ 6000 K, according to the determinations of [59]. Varying this abundance threshold, we checked that above [Ce/Fe] $= 0.6$ the binarity proportion within the sample reached an asymptotic constant value. Additionally, we built a reference sample of 4161 stars within the same temperature range but with [Ce/Fe] < 0.3 dex. These stars are assumed to have normal cerium abundances within the uncertainties. The 0.3 dex threshold is somewhat arbitrary, and it is possible that some extrinsic stars may be inadvertently included in this reference sample. Finally, we defined the golden sample as the subset of the extrinsic sample for which the cerium abundance is most reliable, based on verification using the high-resolution HERMES spectra of a subsample of targets.

As shown in Table 5, the Gaia data reveal that the percentage of detected binaries is 52.44% in the extrinsic sample and increases to 62.50% in the golden sample. In contrast, the reference sample shows a much lower detection rate of just 21.68%, which is the expected binarity rate in this stellar parameter range.

Table 5. Number and proportion of binaries among three different star samples: the "extrinsic" sample, the "reference" sample, and the "golden" sample, as defined in Section 3.

		Extrinsic Sample Proportion (%)	Extrinsic Sample Number (Total: 82 Stars)	Reference Sample Proportion (%)	Reference Sample Number (Total: 4161 Stars)	Golden Sample Proportion (%)	Golden Sample Number (Total: 28 Stars)
Variable radial velocity	Yes	45.12 ± 5.49	37 ± 4.51	14.59 ± 0.55	607 ± 22.77	57.14 ± 9.35	16 ± 2.62
	No	51.22 ± 5.52	42 ± 4.53	80.72 ± 0.61	3359 ± 25.45	39.29 ± 9.23	11 ± 2.58
	Undetermined	3.66 ± 0.23	3 ± 0.19	4.69 ± 0.33	195 ± 13.64	3.57 ± 0.68	1 ± 0.19
Gaia binarity flags	Non binary (NSS = 0)	69.51 ± 5.08	57 ± 4.17	88.18 ± 0.50	3669 ± 20.83	46.43 ± 9.42	13 ± 2.64
	Astrometric binary (NSS = 1)	10.98 ± 3.45	9 ± 2.83	3.58 ± 0.29	149 ± 11.98	17.86 ± 7.23	5 ± 2.02
	Spectroscopic binary (NSS = 2)	9.76 ± 3.28	8 ± 2.69	5.19 ± 0.34	216 ± 14.31	17.86 ± 7.23	5 ± 2.02
	Astrometric and spectroscopic binary (NSS = 3)	9.76 ± 3.28	8 ± 2.69	3.05 ± 0.27	127 ± 11.09	17.86 ± 7.23	5 ± 2.02
Re-normalized v_r error	RUWE $\geq$ 1.4	41.46 ± 5.44	34 ± 4.46	16.46 ± 0.57	685 ± 23.92	50.00 ± 9.45	14 ± 2.65
	RUWE $<$ 1.4	58.54 ± 5.44	48 ± 4.46	83.49 ± 0.58	3474 ± 23.95	50.00 ± 9.45	14 ± 2.65
Union of all binarity indicators		52.44 ± 5.51	43 ± 4.52	21.68 ± 0.64	902 ± 26.58	62.50 ± 9.15	18 ± 2.56

Different statistical tests (namely the Fisher's exact test, the χ^2 test as well as the equality test on large samples) indicate with 99% confidence that we can reject the null hypothesis that the binary proportions are identical in the extrinsic and reference samples. This suggests that the extrinsic sample has an unusually high number of binaries. This finding is consistent with the expectation that cerium-enriched stars, which are not yet evolved to the thermally-pulsing AGB phase, likely acquired their chemical peculiarities through past mass transfer. Consequently, these stars are expected to be binaries [60].

Finally, the scale height above the galactic plane for the extrinsic star sample is measured at 149.64 ± 2.01 pc, compared to 82.37 ± 0.89 pc for the control sample. This difference supports the idea that extrinsic stars belong to an older slightly more metal-poor population, with companions that have already evolved to the white dwarf stage.

We note that among the 82 stars of our extrinsic sample, only eight have previously been identified in the literature as being enriched in heavy elements.

4. Conclusions

This study provides a deep analysis of barium isotopic ratios in selected objects. By employing advanced spectroscopic techniques and high-precision measurements, the barium isotopic ratios have been determined, and they confirm the nucleosynthesis diagnostics obtained from independent methods, e.g., from the abundance profile analysis. In addition, we have shown that large surveys hold significant potential for uncovering a wealth of extrinsic stars, yet to be analyzed. It underlines the relevance of both large spectroscopic surveys with a plethora of objects and detailed studies of key-targets to progress in our understanding of nucleosynthesis processes.

Author Contributions: Conceptualization, S.V.E. and S.G.; methodology, S.V.E., R.G., T.M., S.G., L.S., N.S., M.B. and J.G.; software, R.G., T.M., A.L., S.G., A.C., N.S., L.S. and J.G.; validation, R.G., S.V.E., S.G., L.S., M.B. and A.J.; formal analysis, R.G., T.M. and A.L.; investigation, all; resources, R.G., T.M., D.K., S.G., L.S., A.C., N.S. and J.G.; data curation, R.G., T.M. and S.V.E.; writing—original draft preparation, S.V.E. and R.G.; writing—review and editing, all; visualization, R.G. and A.L.; supervision, S.V.E., S.G., L.S., M.B. and A.J.; project administration, S.V.E. and S.G.; funding acquisition, S.V.E. and S.G. All authors have read and agreed to the published version of the manuscript.

Funding: This research was funded by the Fonds de la Recherche Scientifique (F.R.S.-FNRS) and the Fonds Wetenschap- pelijk Onderzoek,Äö √Ñ√¨Vlaanderen (FWO) under the EOS Projects nr O022818F and O000422F. S.V.E. acknowledges support from ULB Foundation. T.M. receives grants from the BELSPO Belgian federal research program FED-tWIN under the research profile Prf-2020-033_BISTRO. DK acknowledges financial support from ANRF through SURE Grant with file number SUR/2022/000748.

Institutional Review Board Statement: Not applicable.

Informed Consent Statement: Not applicable.

Data Availability Statement: Most data and codes are publicly available. Spectra are available upon requests.

Conflicts of Interest: The authors declare no conflicts of interest. The funders had no role in the design of the study; in the collection, analyses, or interpretation of data; in the writing of the manuscript; or in the decision to publish the results.

Abbreviations

The following abbreviations are used in this manuscript:

TP-AGB	Thermally-Pulsing Asymptotic Giant Branch
(N)LTE	(Non)-Local Thermal Equilibrium

References

1. Arnould, M.; Goriely, S. Astronuclear Physics: A tale of the atomic nuclei in the skies. *Prog. Part. Nucl. Phys.* **2020**, *112*, 103766. [CrossRef]
2. Käppeler, F.; Gallino, R.; Bisterzo, S.; Aoki, W. The *s* process: Nuclear physics, stellar models, and observations. *Rev. Mod. Phys.* **2011**, *83*, 157–193. [CrossRef]
3. Karakas, A. Updated stellar yields from asymptotic giant branch models. *Mon. Not. R. Astron. Soc.* **2010**, *403*, 1413. [CrossRef]
4. Goriely, S.; Siess, L. Sensitivity of the s-process nucleosynthesis in AGB stars to the overshoot model. *Astron. Astrophys.* **2018**, *609*, A29. [CrossRef]
5. Arnould, M.; Goriely, S.; Takahashi, K. The r-process of stellar nucleosynthesis: Astrophysics and nuclear physics achievements and mysteries. *Phys. Repts.* **2007**, *450*, 97–213. [CrossRef]
6. Cowan, J.; Sneden, C.; Lawler, J.; Aprahamian, A.; Wiescher, M.; Langanke, K.; Martínez-Pinedo, G.; Thielemann, F.K. Origin of the heaviest elements: The rapid neutron-capture process. *Rev. Mod. Phys.* **2021**, *93*, 015002. [CrossRef]
7. Gallino, R.; Arlandini, C.; Busso, M.; Lugaro, M.; Travaglio, C.; Straniero, O.; Chieffi, A.; Limongi, M. Evolution and Nucleosynthesis in Low-Mass Asymptotic Giant Branch Stars. II. Neutron Capture and the s-Process. *Astrophys. J.* **1998**, *497*, 388. [CrossRef]
8. Cristallo, S.; Straniero, O.; Gallino, R.; Piersanti, L.; Domínguez, I.; Lederer, M.T. Evolution, Nucleosynthesis, and Yields of Low-Mass Asymptotic Giant Branch Stars at Different Metallicities. *Astrophys. J* **2009**, *696*, 797–820. [CrossRef]
9. Goriely, S.; Bauswein, A.; Janka, H.T. r-process Nucleosynthesis in Dynamically Ejected Matter of Neutron Star Mergers. *Astrophys. J. Lett.* **2011**, *738*, L32. [CrossRef]
10. Abbott, B.P.; Abbott, R.; Abbott, T.D.; Acernese, F.; Ackley, K.; Adams, C.; Adams, T.; Addesso, P.; Adhikari, R.X.; Adya, V.B.; et al. GW170817: Observation of Gravitational Waves from a Binary Neutron Star Inspiral. *Phys. Rev. Lett.* **2017**, *119*, 161101. [CrossRef] [PubMed]
11. Janka, H.T. Explosion Mechanisms of Core-Collapse Supernovae. *Annu. Rev. Nucl. Part. Sci.* **2012**, *62*, 407–451. [CrossRef]
12. Kobayashi, C.; Karakas, A.I.; Lugaro, M. The Origin of Elements from Carbon to Uranium. *Astrophys. J.* **2020**, *900*, 179. [CrossRef]
13. Kobayashi, C.; Mandel, I.; Belczynski, K.; Goriely, S.; Janka, T.H.; Just, O.; Ruiter, A.J.; Vanbeveren, D.; Kruckow, M.U.; Briel, M.M.; et al. Can Neutron Star Mergers Alone Explain the r-process Enrichment of the Milky Way? *Astrophys. J. Lett.* **2023**, *943*, L12. [CrossRef]
14. Lian, J.; Storm, N.; Guiglion, G.; Serenelli, A.; Cote, B.; Karakas, A.I.; Boardman, N.; Bergemann, M. Observational constraints on the origin of the elements - VI. Origin and evolution of neutron-capture elements as probed by the Gaia-ESO survey. *Mon. Not. R. Astron. Soc.* **2023**, *525*, 1329–1341. [CrossRef]
15. Holmbeck, E.M.; Hansen, T.T.; Beers, T.C.; Placco, V.M.; Whitten, D.D.; Rasmussen, K.C.; Roederer, I.U.; Ezzeddine, R.; Sakari, C.M.; Frebel, A.; et al. The R-Process Alliance: Fourth Data Release from the Search for R-process-enhanced Stars in the Galactic Halo. *Astrophys. J. Suppl. Ser.* **2020**, *249*, 30. [CrossRef]
16. Cui, W.Y.; Zhang, B.; Shi, J.R.; Zhao, G.; Wang, W.J.; Niu, P. Possible discovery of the r-process characteristics in the abundances of metal-rich barium stars. *Astron. Astrophys.* **2014**, *566*, A16. [CrossRef]
17. Karinkuzhi, D.; Van Eck, S.; Jorissen, A.; Goriely, S.; Siess, L.; Merle, T.; Escorza, A.; Van der Swaelmen, M.; Boffin, H.M.J.; Masseron, T.; et al. When binaries keep track of recent nucleosynthesis. The Zr-Nb pair in extrinsic stars as an s-process diagnostic. *Astron. Astrophys.* **2018**, *618*, A32. [CrossRef]
18. Karinkuzhi, D.; Van Eck, S.; Goriely, S.; Siess, L.; Jorissen, A.; Merle, T.; Escorza, A.; Masseron, T. Low-mass low-metallicity AGB stars as an efficient i-process site explaining CEMP-rs stars. *Astron. Astrophys.* **2021**, *645*, A61. [CrossRef]
19. den Hartogh, J.W.; Yagüe López, A.; Cseh, B.; Pignatari, M.; Világos, B.; Roriz, M.P.; Pereira, C.B.; Drake, N.A.; Junqueira, S.; Lugaro, M. Barium stars as tracers of s-process nucleosynthesis in AGB stars. II. Using machine learning techniques on 169 stars. *Astron. Astrophys. 2023* **2023**, *672*, A143. [CrossRef]

20. Karinkuzhi, D.; Van Eck, S.; Goriely, S.; Siess, L.; Jorissen, A.; Choplin, A.; Escorza, A.; Shetye, S.; Van Winckel, H. Does the i-process operate at nearly solar metallicity? *Astron. Astrophys.* **2023**, *677*, A47. [CrossRef]
21. Beers, T.C.; Christlieb, N. The Discovery and Analysis of Very Metal-Poor Stars in the Galaxy. *Annu. Rev. Astron. Astrophys.* **2005**, *43*, 531–580. [CrossRef]
22. Masseron, T.; Johnson, J.A.; Plez, B.; van Eck, S.; Primas, F.; Goriely, S.; Jorissen, A. A holistic approach to carbon-enhanced metal-poor stars. *Astron. Astrophys.* **2010**, *509*, A93. [CrossRef]
23. Hansen, C.J.; Hansen, T.T.; Koch, A.; Beers, T.C.; Nordström, B.; Placco, V.M.; Andersen, J. Abundances and kinematics of carbon-enhanced metal-poor stars in the Galactic halo. A new classification scheme based on Sr and Ba. *Astron. Astrophys.* **2019**, *623*, A128. [CrossRef]
24. Hansen, T.T.; Andersen, J.; Nordström, B.; Beers, T.C.; Placco, V.M.; Yoon, J.; Buchhave, L.A. The role of binaries in the enrichment of the early Galactic halo. III. Carbon-enhanced metal-poor stars - CEMP-s stars. *Astron. Astrophys.* **2016**, *588*, A3. [CrossRef]
25. Gull, M.; Frebel, A.; Cain, M.G.; Placco, V.M.; Ji, A.P.; Abate, C.; Ezzeddine, R.; Karakas, A.I.; Hansen, T.T.; Sakari, C.; et al. The R-Process Alliance: Discovery of the First Metal-poor Star with a Combined r- and s-process Element Signature. *Astrophys. J.* **2018**, *862*, 174. [CrossRef]
26. Hampel, M.; Stancliffe, R.J.; Lugaro, M.; Meyer, B.S. The Intermediate Neutron-capture Process and Carbon-enhanced Metal-poor Stars. *Astrophys. J.* **2016**, *831*, 171. [CrossRef]
27. Iben, I., Jr.; Renzini, A. Asymptotic giant branch evolution and beyond. *Annu. Rev. Astron. Astrophys.* **1983**, *21*, 271–342. [CrossRef]
28. Jonsell, K.; Barklem, P.S.; Gustafsson, B.; Christlieb, N.; Hill, V.; Beers, T.C.; Holmberg, J. The Hamburg/ESO R-process enhanced star survey (HERES). III. HE 0338-3945 and the formation of the r + s stars. *Astron. Astrophys.* **2006**, *451*, 651–670. [CrossRef]
29. Cowan, J.J.; Rose, W.K. Production of ^{14}C and neutrons in red giants. *Astrophys. J.* **1977**, *212*, 149–158. [CrossRef]
30. Serenelli, A. Nucleosynthesis in Low Mass Very Metal Poor AGB Stars. In *Chemical Abundances and Mixing in Stars in the Milky Way and Its Satellites*; Randich, S., Pasquini, L., Eds.; Springer: Berlin/Heidelberg, Germany, 2006; p. 322. [CrossRef]
31. Choplin, A.; Siess, L.; Goriely, S. The intermediate neutron capture process. I. Development of the i-process in low-metallicity low-mass AGB stars. *Astron. Astrophys.* **2021**, *648*, A119. [CrossRef]
32. Choplin, A.; Siess, L.; Goriely, S. The intermediate neutron-capture process in AGB stars. *Eur. Phys. J. Web Conf.* **2023**, *279*, 07001. [CrossRef]
33. Choplin, A.; Siess, L.; Goriely, S. The intermediate neutron capture process III. The i-process in AGB stars of different masses and metallicities without overshoot. *Astron. Astrophys.* **2022**, *667*, A155. [CrossRef]
34. Martinet, S.; Choplin, A.; Goriely, S.; Siess, L. The intermediate neutron capture process. IV. Impact of nuclear model and parameter uncertainties. *Astron. Astrophys.* **2024**, *684*, A8. [CrossRef]
35. Choplin, A.; Goriely, S.; Siess, L.; Martinet, S. Synthesis of actinides and short-lived radionuclides during i-process nucleosynthesis in AGB stars. *Eur. Phys. J.* **2025**, *in press*.
36. Goriely, S. Uncertainties in the solar system r-abundance distribution. *Astron. Astrophys.* **1999**, *342*, 881–891.
37. Bisterzo, S.; Travaglio, C.; Gallino, R.; Wiescher, M.; Kaeppeler, F. Galactic Chemical Evolution and Solar s-process Abundances: Dependence on the 13C-pocket Structure. *Astrophys. J* **2014**, *787*, 10. [CrossRef]
38. Prantzos, N.; Abia, C.; Cristallo, S.; Limongi, M.; Chieffi, A. Chemical evolution with rotating massive star yields II. A new assessment of the solar s- and r-process components. *Mon. Not. R. Astron. Soc.* **2020**, *491*, 1832. [CrossRef]
39. Mashonkina, L.; Gehren, T.; Bikmaev, I. Barium abundances in cool dwarf stars as a constraint to s- and r-process nucleosynthesis. *Astron. Astrophys.* **1999**, *343*, 519–530.
40. Mashonkina, L.; Gehren, T. Heavy element abundances in cool dwarf stars: An implication for the evolution of the Galaxy. *Astron. Astrophys.* **2001**, *376*, 232–247. [CrossRef]
41. Mashonkina, L.; Zhao, G. Barium even-to-odd isotope abundance ratios in thick disk and thin disk stars. *Astron. Astrophys.* **2006**, *456*, 313–321. [CrossRef]
42. Mashonkina, L.; Christlieb, N. The Hamburg/ESO R-process Enhanced Star survey (HERES). IX. Constraining pure r-process Ba/Eu abundance ratio from observations of r-II stars. *Astron. Astrophys.* **2014**, *565*, A123. [CrossRef]
43. Magain, P.; Zhao, G. Barium isotopes in the very metal-poor star HD 140283. *Astron. Astrophys.* **1993**, *268*, L27–L29.
44. Lambert, D.L.; Allende Prieto, C. The isotopic mixture of barium in the metal-poor subgiant HD 140283. *Mon. Not. R. Astron. Soc.* **2002**, *335*, 325–334. [CrossRef]
45. Collet, R.; Asplund, M.; Nissen, P.E. The Barium Isotopic Abundance in the Metal-Poor Star HD140283. *Publ. Astron. Soc. Aust.* **2009**, *26*, 330–334. [CrossRef]
46. Gallagher, A.J.; Ryan, S.G.; García Pérez, A.E.; Aoki, W. The barium isotopic mixture for the metal-poor subgiant star HD 140283. *Astron. Astrophys.* **2010**, *523*, A24. [CrossRef]
47. Gallagher, A.J.; Ludwig, H.G.; Ryan, S.G.; Aoki, W. A three-dimensional hydrodynamical line profile analysis of iron lines and barium isotopes in HD 140283. *Astron. Astrophys.* **2015**, *579*, A94. [CrossRef]
48. Meng, X.Y.; Cui, W.Y.; Shi, J.R.; Jiang, X.H.; Zhao, G.; Zhang, B.; Li, J. The odd-isotope fractions of barium in CEMP-r/s star HE 0338-3945 and r-II star CS 31082-001. *Astron. Astrophys.* **2016**, *593*, A62. [CrossRef]
49. Wenyuan, C.; Xiaohua, J.; Jianrong, S.; Gang, Z.; Bo, Z. The Odd Isotope Fractions of Barium in the Strongly r-process-enhanced (r-II) Stars. *Astrophys. J.* **2018**, *854*, 131. [CrossRef]

50. Short, C.I.; Hauschildt, P.H. NLTE Strontium and Barium in Metal-poor Red Giant Stars. *Astrophys. J.* **2006**, *641*, 494–503. [CrossRef]
51. Raskin, G.; van Winckel, H.; Hensberge, H.; Jorissen, A.; Lehmann, H.; Waelkens, C.; Avila, G.; de Cuyper, J.P.; Degroote, P.; Dubosson, R.; et al. HERMES: A high-resolution fibre-fed spectrograph for the Mercator telescope. *Astron. Astrophys.* **2011**, *526*, A69. [CrossRef]
52. Tomkin, J.; Lambert, D.L.; Edvardsson, B.; Gustafsson, B.; Nissen, P.E. HR 107—An F-type mild barium dwarf star. *Astron. Astrophys.* **1989**, *219*, L15–L18.
53. Sneden, C.; Lawler, J.E.; Cowan, J.J.; Ivans, I.I.; Den Hartog, E.A. New Rare Earth Element Abundance Distributions for the Sun and Five r-Process-Rich Very Metal-Poor Stars. *Astrophys. J. Suppl. Ser.* **2009**, *182*, 80–96. [CrossRef]
54. Hansen, T.; Hansen, C.J.; Christlieb, N.; Beers, T.C.; Yong, D.; Bessell, M.S.; Frebel, A.; García Pérez, A.E.; Placco, V.M.; Norris, J.E.; et al. An Elemental Assay of Very, Extremely, and Ultra-metal-poor Stars. *Astrophys. J.* **2015**, *807*, 173. [CrossRef]
55. Amarsi, A.M.; Nordlander, T.; Barklem, P.S.; Asplund, M.; Collet, R.; Lind, K. Effective temperature determinations of late-type stars based on 3D non-LTE Balmer line formation. *Astron. Astrophys.* **2018**, *615*, A139. [CrossRef]
56. Giribaldi, R.E.; Ubaldo-Melo, M.L.; Porto de Mello, G.F.; Pasquini, L.; Ludwig, H.G.; Ulmer-Moll, S.; Lorenzo-Oliveira, D. Accurate effective temperature from Hα profiles. *Astron. Astrophys.* **2019**, *624*, A10. [CrossRef]
57. Giribaldi, R.E.; Van Eck, S.; Merle, T.; Jorissen, A.; Krynski, P.; Planquart, L.; Valentini, M.; Chiappini, C.; Van Winckel, H. TITANS metal-poor reference stars. II. Red giants and CEMP stars. *Astron. Astrophys.* **2023**, *679*, A110. [CrossRef]
58. Gerber, J.M.; Magg, E.; Plez, B.; Bergemann, M.; Heiter, U.; Olander, T.; Hoppe, R. Non-LTE radiative transfer with Turbospectrum. *Astron. Astrophys.* **2023**, *669*, A43. [CrossRef]
59. Contursi, G.; de Laverny, P.; Recio-Blanco, A.; Spitoni, E.; Palicio, P.A.; Poggio, E.; Grisoni, V.; Cescutti, G.; Matteucci, F.; Spina, L.; et al. The cerium content of the Milky Way as revealed by Gaia DR3 GSP-Spec abundances. *Astron. Astrophys.* **2023**, *670*, A106. [CrossRef]
60. McClure, R.D.; Woodsworth, A.W. The Binary Nature of the Barium and CH Stars. III. Orbital Parameters. *Astrophys. J.* **1990**, *352*, 709. [CrossRef]